Record-Low Spatial Mode Dispersion and Ultra-Low Loss Coupled Multi-Core Fiber for Ultra-Long-Haul Transmission

Tetsuya Hayashi, *Member, IEEE, Member, OSA*, Yoshiaki Tamura, Takemi Hasegawa, *Member, IEEE*, and Toshiki Taru

(Post-Deadline)

***Abstract*—Newly developed 125-μm-cladding coupled four-core fibers realized the record-low spatial mode dispersion (SMD) of 3.14 $\pm$ 0.17 ps/$\sqrt{}$km over C-band and the ultra-low attenuation of 0.158 dB/km at 1550 nm, both of which are the lowest ever reported among the optical fibers for the space-division multiplexed transmission. The SMD was observed to be proportional to the fiber bend curvature, i.e., inversely proportional to the bend radius, and the SMD of 3.14 $\pm$ 0.17 ps/$\sqrt{}$km was measured at the bending radius of $\sim$31 cm. By assuming the 3.14-ps/$\sqrt{}$km SMD accumulation, the tap count of the multiple-input multiple-output digital signal processing for the crosstalk compensation is estimated to be only 63 taps for covering 99.99% power of the impulse response after 10 000-km propagation when the 25-GBaud (50-GHz sampling) is assumed. The present results demonstrate the strong applicability of the coupled multicore fiber to the ultralong-haul submarine transmission system.**

***Index Terms*—Coupled-core MCF, coupled MCF, MCF, multi-core fibers, optical fiber communication, optical fibers, SDM, space division multiplexing.**

I. Introduction

THE transmission capacity through the single-mode fiber (SMF) had reached its fundamental limit of around 100 Tb/s/fiber in research activities [1], [2], and the spatial division multiplexing (SDM) technologies are being intensively studied to overcome the capacity limit [3]. In deployed transpacific transmission systems, the system capacity has been exponentially increasing as shown in Fig. 1, and the latest system can transmit full-duplex 60 Tb/s signal with six pairs of fibers (each fiber supports 10 Tb/s) in one cable [4]. With an extrapolation from the capacity growth in Fig. 1, demands of full-duplex multi-petabits/s systems in 2025 can be estimated.

To realize such an ultra-high capacity system, we have to increase the fiber pair count in a cable and/or the capacity of each fiber, e.g., 12 fiber pairs where each fiber transmit $\sim$80 Tb/s can realize the full-duplex $\sim$1-Pb/s transmission. One may think that 12 fiber pairs (24 fibers) are very few compared with ultra-high-count terrestrial cables; however, the fiber count increase is very challenging in submarine cables, because a thicker/heavier cable significantly increases the cable installation cost due to the limited loading capacities of installation ships. The fiber identification is another difficulty for the high-count jelly-filled loose-tube submarine cable. Transmitting $\sim$80 Tb/s in a SMF over transoceanic distance is also challenging, which requires the exponential improvement of the optical signal-to-noise ratio (OSNR), according to the Shannon limit. Hero transmission experiments in research [2], [5], [6] indicate the capacity limit of the SMF system around 50 Tb/s for 10,000-km reach, as shown in Fig. 2, even with advanced ultra-low-loss and low-nonlinearity fibers.

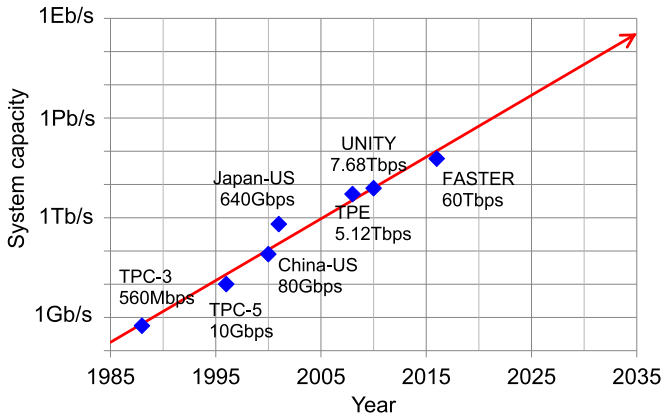

Fig. 1. The capacity growth of transpacific fiber optic transmission systems.

In such a situation, the "capacity crunch" of the transoceanic SMF transmission system is likely to become a reality in the next ten years, and the SDM fiber is a possible solution that can simply multiply the spatial channel count whereby using the conventional submarine cable. However, to use in the ultra-long-haul submarine system, the SDM fiber has to realize ultra-low loss for OSNR improvement, higher spatial-mode density for increasing the spatial channel count within the standard 125-μm cladding, and lower differential group delay (DGD) between spatial modes (spatial mode dispersion (SMD)) for suppressing the digital signal processing (DSP) complexity.

Manuscript received June 28, 2016; revised September 13, 2016; accepted September 22, 2016. Date of publication September 26, 2016; date of current version February 13, 2017.

The authors are with the Optical Communications Laboratory, Sumitomo Electric Industries, Ltd., Sakae-ku 244-8588, Japan (e-mail: t-hayashi@sei.co.jp; tamura-yoshiaki@sei.co.jp; hase@sei.co.jp; taru-toshiki@sei.co.jp).

Color versions of one or more of the figures in this paper are available online at http://ieeexplore.ieee.org.

Digital Object Identifier 10.1109/JLT.2016.2614000

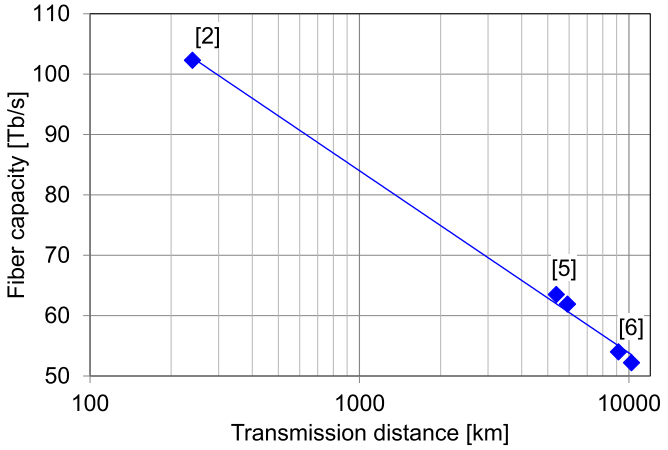

Fig. 2. The SMF transmission capacities and distances demonstrated in the hero experiments reported in [2], [5], [6].

In this paper, we describe a coupled-core multi-core fiber (CC-MCF) having four pure-silica cores with enlarged effective areas (A_{eff}) of 112 μm^2 within the standard 125-μm cladding [7], with additional measurement results. The fabricated CC-MCF realized the SMD of 3.14 $\pm$ 0.17 ps/$\sqrt{}$km—further improved from [7]— over the C-band and the average attenuation of 0.158 dB/km at 1550 nm, both of which show the lowest values ever reported among the optical fibers for the SDM transmission.

II. Fiber Design

In order to achieve ultra-low loss and low SMD, we employed a CC-MCF where cores are arranged close to each other. The CC-MCF can provide higher spatial channel density compared with the uncoupled MCF [8], [9], and can also induce the strong random mode coupling that can suppress the accumulations of the DGD/SMD [9], [10], the mode dependent loss/gain (MDL/MDG) [11], and the nonlinear impairments [12], [13]. The DGD/SMD suppression is a critical factor for reducing the calculation complexity in the multiple-input-multiple-output (MIMO) DSP for the crosstalk compensation. The CC-MCF has potential to simultaneously realize low DGD/SMD and ultra-low loss comparable to the lowest loss realized in the SMF (cf. [14]–[16]), because the CC-MCF can suppress the DGD/SMD with simple step-index-type pure-silica cores thanks to the random coupling [9], [10], [17], in contrast to the single-core few/multi-mode fiber (FMF/MMF) that needs a GeO_2-doped precisely-controlled graded-index-type core for the DGD suppression.

In design of the CC-MCF, we basically dealt with the core mode properties of the CC-MCF because each eigenmode of the whole coupled-core waveguide structure is localized in each core due to the index mismatch induced by the fiber bend, except for the index-matching points discretized by the fiber twist [9]. We designed the CC-MCF as shown in Fig. 3, based on the refractive index profile of the ultra-low-loss (ULL) pure-silica-core (PSC) SMF with the enlarged A_{eff} of 112 μm^2 (PSCF-110 [14]). A ring core is surrounded by a depressed inner cladding for simultaneously increasing the A_{eff} and suppressing the macrobend loss, and the depressed cladding is surrounded by an

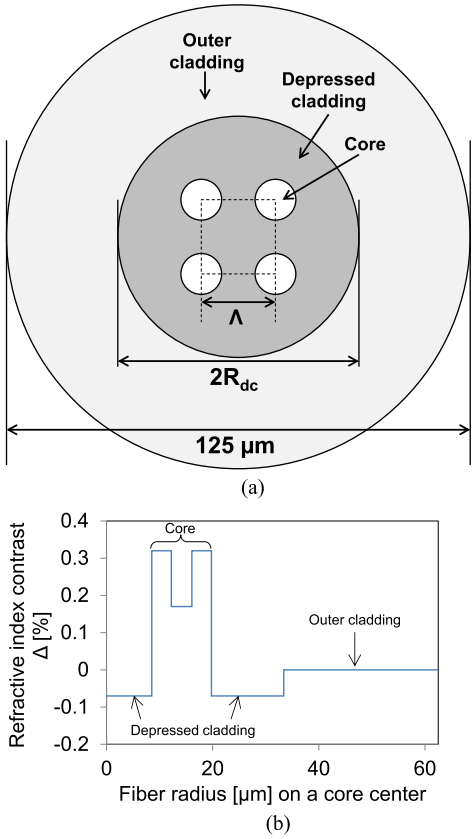

Fig. 3. Design of the CC-MCF: (a) cross-section (darker represents lower index), and (b) refractive index profile on a radial line on a core center.

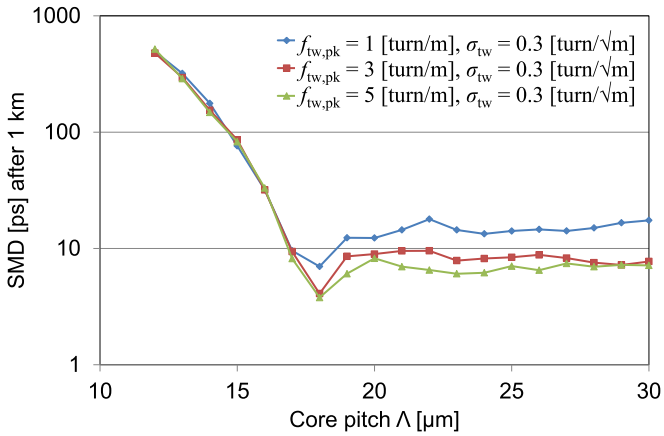

Fig. 4. The relationship between the core pitch and the simulated SMD at the wavelength of 1550 nm, the R_b of 15 cm, and various twisting conditions.

outer cladding with higher refractive index for shortening the cable cutoff wavelength (λ_{cc}). In the CC-MCF design, the core index profile is identical to each other, and the common depressed cladding is shared by all the cores. The cores were arranged on the square lattice.

The core pitch Λ was designed to be 20 μm for realizing adequate random couplings due to the bends and twists [9], by assuming a spun fiber. To confirm if the adequate couplings occur with the designed Λ, we numerically simulated the SMD of four-core fiber with the designed core for different Λ from 12 to 30 μm, using the method presented in [18]. The results

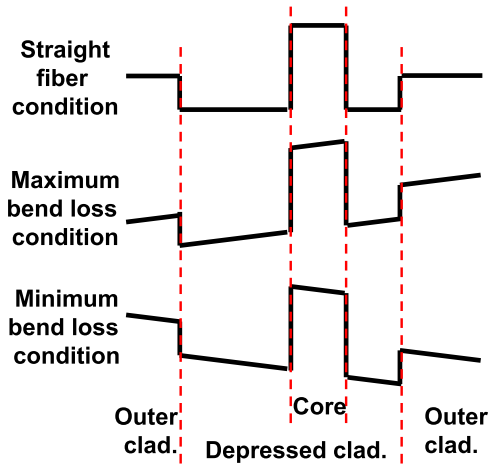

Fig. 5. A schematic illustration showing bend-affected equivalent refractive index profiles of a core located apart from the center of the depressed cladding.

are shown in Fig. 4. Here, the SMD was defined as the statistical average of the maximum difference of the group delays of the principal modes [19], which was calculated using the non-orthogonal coupled mode theory based on the core modes [20] that can hold even when the core modes are strongly coupled. The bend radius $R_{\rm b}$ in the calculation was set to be 15 cm by assuming a 14-cm-radius bobbin and winding thickness of the fiber. In this calculation, we assumed the fiber twist consists of a non-random component which is a sinusoidally-modulated bidirectional twist whose peak rate $f_{\rm tw,pk}$ is 1, 3, or 5 [turn/m] and a random component whose twist rate is an additive white Gaussian noise with the standard deviation $\sigma_{\rm tw}$ of 0.3 [turn/$\sqrt{\rm m}$]. The SMD was simulated by Monte-Carlo simulation with 25 instances of the random twist component. According to the simulation results, the SMD is expected to be well suppressed by the twists when the Λ is $\sim$18 μm or longer in the case of the designed core.

The outer cladding diameter of the CC-MCF was designed to be 125 μm, which is the same as the standard optical fibers. The depressed cladding diameter ($2R_{\rm dc}$) and the refractive index contrast between the depressed cladding and the outer cladding were designed to suppress the $\lambda_{\rm cc}$ less than 1530 nm, and macrobend loss less than 0.2 dB/turn at λ of 1550 nm and the $R_{\rm b}$ of 15 mm. As each core is located apart from the center of the depressed cladding, the macrobend loss was calculated in the maximum bend loss condition, and the $\lambda_{\rm cc}$ in the minimum bend loss condition (see Fig. 5 for the maximum/minimum bend loss conditions). The designed optical characteristics of the core mode are summarized in Table I.

TABLE I
DESIGNED CORE-MODE CHARACTERISTICS AT 1550 NM.

Items	Values
$A_{\rm eff}$	112 μm^2
$\lambda_{\rm cc}$	$\leq$ 1490 nm
Bend loss at $R_{\rm b}$ = 15 mm	$\leq$ 0.2 dB/turn
Chromatic dispersion	20.9 ps/(nm·km)
Dispersion slope	0.060 ps/(nm^2·km)

III. Fabrication Results

According to the above design, we fabricated a CC-MCF. Table II shows the optical properties of four samples of the fabricated CC-MCF, and Figs. 6 and 7 show the cross section and the average attenuation spectra, respectively. The measured Λ values were from 19.5 to 19.8 μm. The CC-MCF was twisted in alternating direction. We have not succeeded in measuring the actual twist rate of the CC-MCF because of difficulty in measurement, but we suppose the peak twist rate is in the range of 1 to 5 turns/m, based on our past measurement experiences of twisted slightly elliptic fibers.

The attenuation was measured using the cutback and backscattering methods [21]. Because the inter-core crosstalk was so strong that the powers in the core modes can be completely mixed within less than one-meter propagation, the measured attenuation was averaged over the modes and thus we measured average attenuation in both methods. The lowest average attenuation at 1550 nm observed in the cutback method was 0.158 dB/km, and is much lower than those of the previously reported MCFs (0.177 dB/km in the CC-MCF [9], 0.168 dB/km in the uncoupled MCF [22]), and approaching to those of the ultra-low-loss SMFs (0.147–0.154 dB/km) [14]–[16], thanks to the ULL PSC technology [14] which was also applied recently to an uncoupled MCF resulting in the loss as low as 0.161 dB/km [23]. The difference of average attenuations between the cutback and backscattering methods in the cases of Samples 1 and 2 may be due to slight excess losses induced near the output end of the samples.

The $\lambda_{\rm cc}$ was measured using multimode reference method [21]. The $\lambda_{\rm cc}$ of the higher-order modes, except the modes corresponding to the fundamental core modes, was measured to be $<$1480 nm, as shown in Table II.

The chromatic dispersion (CD) averaged over the spatial modes was measured using the conventional modulation phase shift method [24]. In the CD measurement, we launched and received the light into and from a core. The measured spectra of the relative group delays (GDs) and CDs averaged over modes are shown in Fig. 8. The fitting curves represent the five-term Sellmeier equation [21], fitted to the relative GD spectra. Though the measured CD spectra are somewhat noisy, the CDs and their slopes obtained from the fitting curves agreed well with the design, as shown in Table II. The noise in the measured CD is considered because the DGD and random coupling induced interference fringe on the impulse response, and the GD with peak intensity was fluctuated.

The marcrobend loss at $R_{\rm b}$ = 15 mm was measured to be lower than 0.1 dB/turn at 1550 nm.

The $A_{\rm eff}$ were not able to be measured due to the strong random mode mixing. Evaluation method developments would be necessary for the $A_{\rm eff}$ evaluation. However, we expect the $A_{\rm eff}$ would be similar to their design values, since the measured values of the other parameters agreed with their design values.

IV. Spatial Mode Dispersion Measurements and Discussion

The spatial mode dispersion (SMD) was measured in the range of 1520 to 1580 nm using the method similar to

TABLE II
MEASURED OPTICAL CHARACTERISTICS AT 1550 NM OF THE FABRICATED CC-MCF.

Sample	Length [km]	Average attenuation [dB/km]		λ_{cc} [nm]	CD [ps/(nm·km)]	CD slope [ps/(nm^2·km)]	Bend loss [dB/turn] at R_b = 15 mm
		Cutback	Backscattering				
Design	n/a	n/a	n/a	<1490	20.9	0.060	≤ 0.2
Sample-1	17.3	0.158	0.157	1469	20.1	0.061	0.064
Sample-2	24.2	0.161	0.159	1468	20.1	0.063	0.069
Sample-3	30.1	0.160	0.160	1472	20.1	0.061	0.046
Sample-4	41.2	0.159	0.159	1473	20.0	0.060	0.058

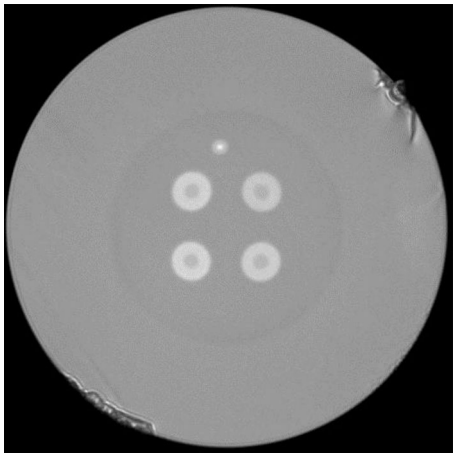

Fig. 6. A cross section of a fabricated CC-MCF [7].

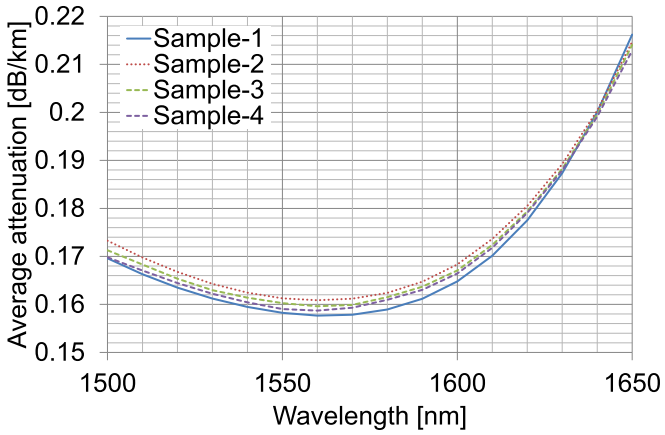

Fig. 7. The average attenuation spectra of the fabricated CC-MCFs.

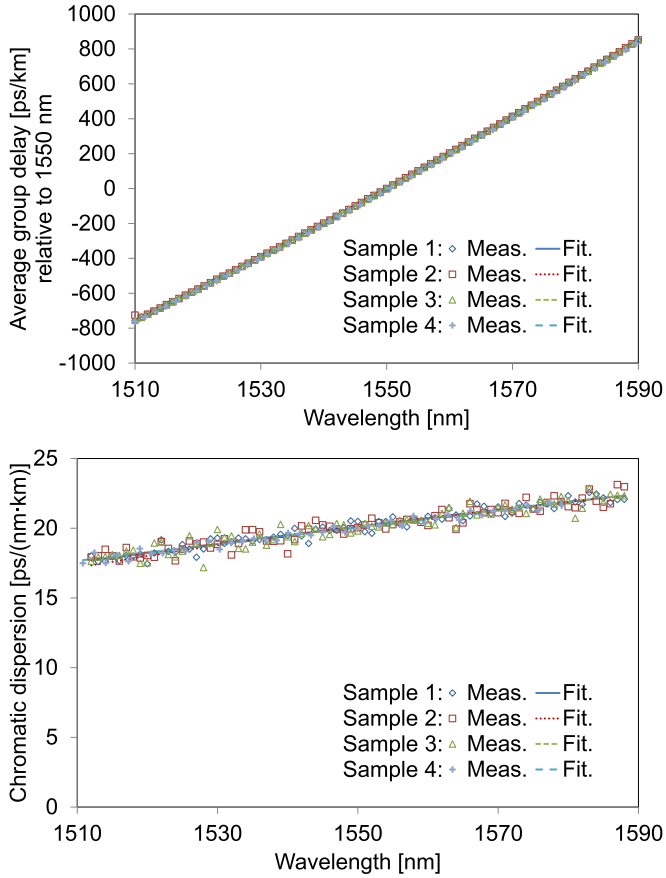

Fig. 8. The spectra of (upper) the relative GD and (lower) the CD of the fabricated CC-MCFs. The measured marks in the relative GD spectra overlap the 5-term Sellmeier fitting curves. The measured marks in the CD spectra were somewhat noisy because of the DGD and random coupling.

the fixed analyzer technique—sometimes also referred to as the wavelength scanning technique/method— with Fourier analysis for the polarization mode dispersion (PMD) measurement [25], after Sakamoto *et al.* [17]. The measurement setup is shown in Fig. 9, and basically the same with the setup for measuring the crosstalk spectrum by the wavelength-scanning method, described in [26]. We measured a transmission spectrum of each core from 1520 to 1580 nm with the 5-pm step using a tunable light source with ∼100-kHz linewidth. The measured transmission spectrum was Fourier-transformed, and the probability distribution of the DGD $\Delta\tau$ was obtained as the result of the Fourier transform. Before the Fourier transform, the transmission spectrum with equal wavelength interval was converted to the spectrum with equal frequency interval by cubic spline interpolation, its DC offset was removed, and the appropriate window function was applied (the Nuttall-defined minimum 4-term Blackman-Harris window [27] was used in this study). The measured DGD $\Delta\tau$ distribution was Gaussian-distributed as shown in Fig. 10. The SMD was defined as the square root of the second moment of the DGD distribution, i.e., the standard deviation σ_R of the autocorrelation function of the impulse response, as with the case of the PMD measurement [25]. The σ_R is twice the standard deviation σ_I of the impulse

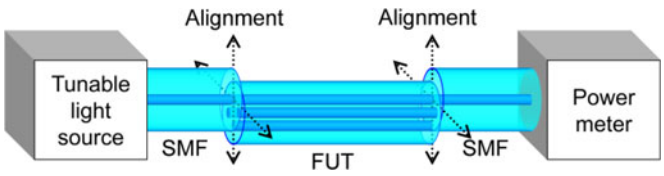

Fig. 9. The schematic experimental setup for observing the transmission spectrum of a core of the CC-MCF (FUT: fiber under test), for measuring the SMD in the similar way to the fixed analyzer method for PMD measurement.

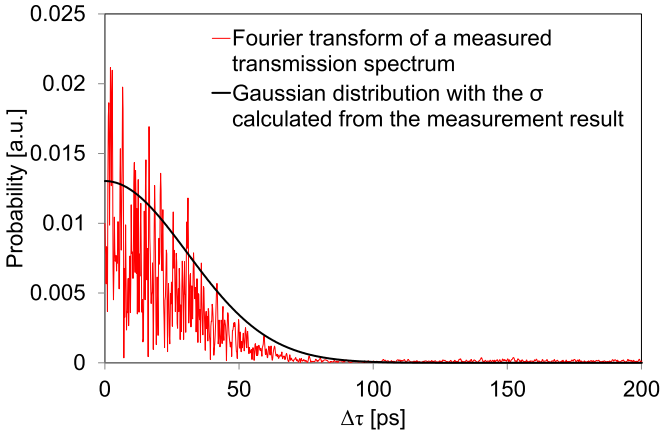

Fig. 10. An example of measured DGD distributions.

TABLE III
SPATIAL MODE DISPERSION OF THE FABRICATED CC-MCF.

Sample	Length [km]	SMD [ps]*	SMD coeff. [ps/√km]*
Sample-0	2.975	12.05 ± 0.31	7.99 ± 0.18
Sample-1	17.31	26.05 ± 0.48	6.26 ± 0.12
Sample-2	24.24	32.28 ± 0.50	6.56 ± 0.10
Sample-3	30.06	33.41 ± 0.02	6.09 ± 0.00
Sample-4	41.22	36.67 ± 0.52	5.71 ± 0.08

* The samples were wound on 140-mm-radius bobbin, and measurement wavelength range was 1520–1580 nm. Each value shows the average ± the standard error.

response [28]—σ_{I} corresponds to σ values in [9], [10]. The measured SMD $\langle \Delta\tau \rangle$ values and the SMD evolution over the fiber length are shown in Table III and Fig. 11, respectively. The SMD of the samples agreed well with the square-root curve having the SMD coefficient of 6.1 ps/$\sqrt{}$km, calculated from $[(\sum \sigma_{\mathrm{R}}^2)/(\sum L)]^{1/2}$ of Samples 1–4.

Next, we obtained 1-km pieces from Sample 4 and investigated the dependence of the SMD on the fiber bending radius R_{b}. We measured the SMD at R_{b} of 8 cm, 14 cm, and 31 cm. The results are shown in Table IV and Fig. 12. The linear proportionality of the SMD on the fiber curvature $(1/R_{\mathrm{b}})$ was clearly observed, as shown in Fig. 12. The SMD at R_{b} of 31 cm was further suppressed to be 3.14 ± 0.17 ps/$\sqrt{}$km.

The SMDs measured over C-band with the fabricated CC-MCFs are much lower than the values reported in the CC-MCFs [10], [17] and C-band DGD in FMFs [29]–[31] in the long-haul region longer than tens of km, as shown in Fig. 13.

Based on the measurement results, the SMD after 10,000-km transmission is expected to be 6.1 × 10^2 ps for the 6.1-ps/$\sqrt{}$km case and to be 3.14 × 10^2 ps for the 3.14-ps/$\sqrt{}$km case, sufficiently low for suppressing MIMO calculation complexity. Assuming a 25-GBaud symbol rate (50-GHz sampling), the required tap counts for MIMO DSP for the transmission over the fabricated CC-MCF for covering most of the power of the impulse responses were estimated for the 6.1-ps/$\sqrt{}$km and 3.14-ps/$\sqrt{}$km cases, as shown in Fig. 14 and Table V. Even after 10,000-km transmission, the required tap count can be

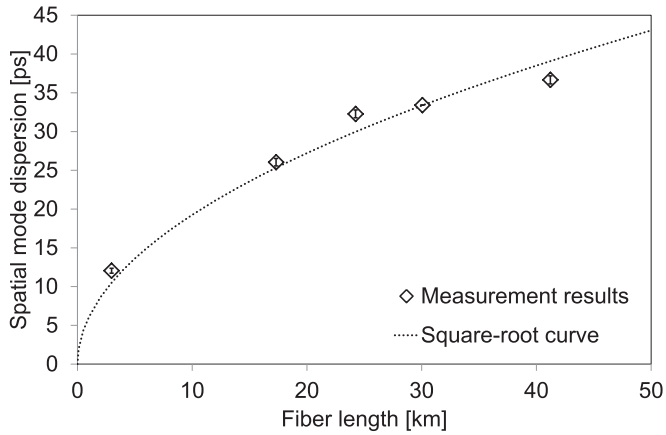

Fig. 11. The SMD of the fabricated CC-MCFs (Error bars represent the standard errors of the measurements with different core launching).

TABLE IV
THE EFFECT OF THE FIBER BEND RADIUS ON THE SPATIAL MODE DISPERSION OF THE FABRICATED CC-MCF.

Bend radius [cm]	Length [km]	SMD [ps]*
8	1.00	15.05 ± 0.11
14	1.00	8.55 ± 0.21
31	1.00	3.14 ± 0.17

* Measurement wavelength range was 1520–1580 nm. Each value show the average ± the standard error.

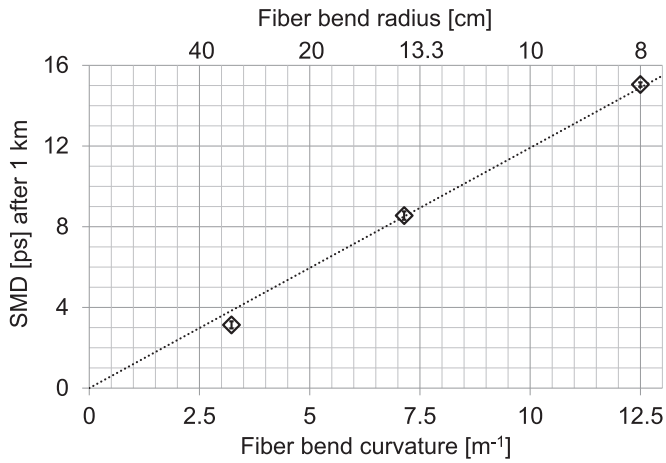

Fig. 12. The relationship between the fiber bend curvature and the SMD of 1-km pieces obtained from the fabricated CC-MCF. (Error bars represent the standard errors of the measurements with different core launching. The line is the linear regression from the origin).

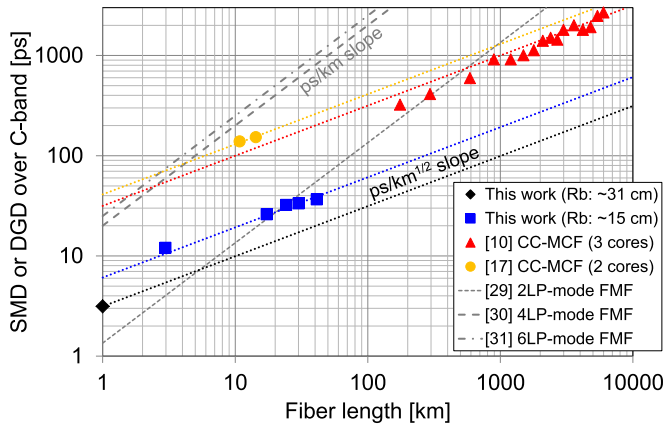

Fig. 13. A comparison of the SMD or DGD over C-band between the fabricated CC-MCF and SDM fibers reported in [10], [17], [29–31] (The marks and the dotted lines for the CC-MCFs are the measured values and the regression lines. DGDs of the FMFs are the estimated values of the DGD-compensated links with the optimized positive/negative-DGD fiber ratios by interpolating the measured DGDs).

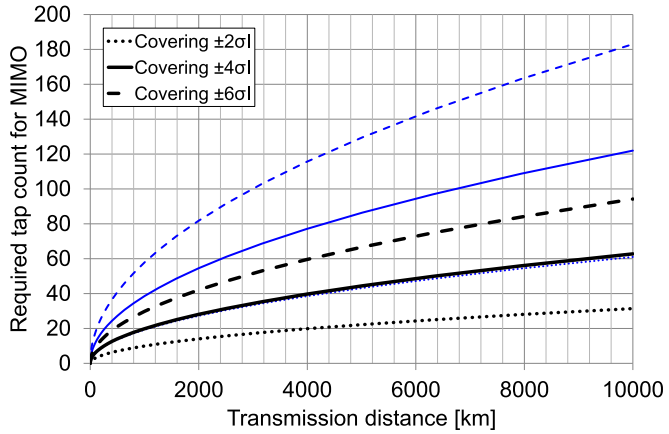

Fig. 14. The required tap count for MIMO DSP for the fabricated CC-MCF. (Black thicker curves: 3.14 ps/$\sqrt{}$km, blue thinner curves: 6.1 ps/$\sqrt{}$km).

TABLE V
THE REQUIRED TAP COUNT FOR MIMO DSP FOR THE FABRICATED CC-MCF AFTER 10,000-KM TRANSMISSION FOR COVERING THE MOST OF THE IMPULSE RESPONSES.

Covering interval	Uncovered power of impulse response	Required tap count	
		6.1-ps/$\sqrt{}$km SMD case	3.14-ps/$\sqrt{}$km SMD case
$\pm 2\sigma_{\mathrm{I}} = 2\sigma_{\mathrm{R}}$	$\sim 4.6 \times 10^{-2}$	61	32
$\pm 4\sigma_{\mathrm{I}} = 4\sigma_{\mathrm{R}}$	$\sim 6.3 \times 10^{-7}$	1.2×10^{2}	63
$\pm 6\sigma_{\mathrm{I}} = 6\sigma_{\mathrm{R}}$	$\sim 2.0 \times 10^{-9}$	1.8×10^{2}	95

quite a reasonable value for suppressing the MIMO calculation complexity.

A remaining concern on the SMD is its degradation due to tight bends or too loose (nearly straight) bends of the fibers in actual deployed conditions. The tight bends can be applied to the fibers as small-radius spools for slack fiber storage in repeaters.

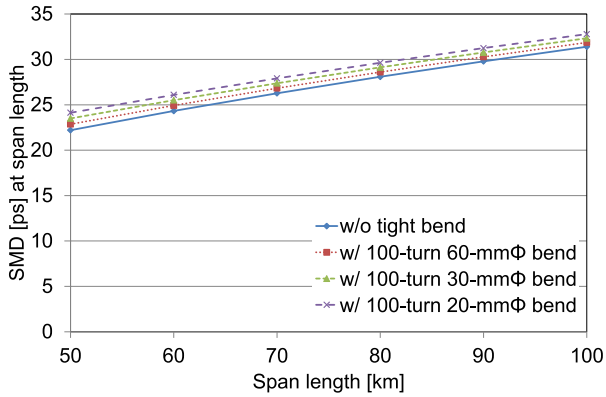

Fig. 15. The estimated SMDs for one span with/without tight bend in a repeater, as a function of the span length. Except the tightly bent portion, the SMD coefficient of 3.14 ps/$\sqrt{}$km was assumed.

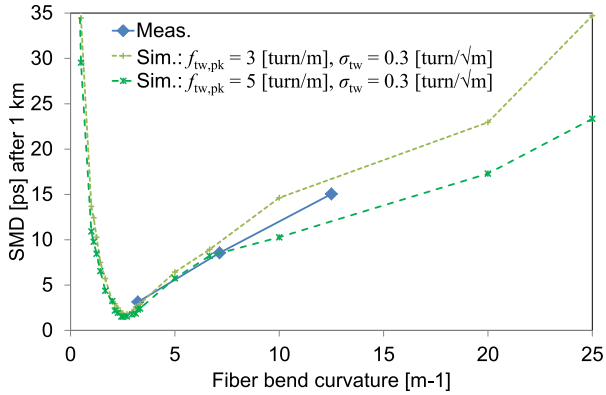

Fig. 16. The simulated SMDs at 1550 nm after 1-km propagation, as a function of the fiber curvature. The measured results are also plotted together.

Thus, we estimated the SMD after one span CC-MCF propagation including one repeater, based on the proportionality of the SMD on the bend curvature in Fig. 12. We assumed the SMD coefficient of 3.14 ps/$\sqrt{}$km except for the small spool in the repeater. The small spool was assumed as the 100-turn bend with the diameter of 60 mm, 30 mm, or 20 mm. As shown in Fig. 15, slight SMD increases were observed due to the small spool, but are considered to be manageable in the MIMO DSP. On the other hand, optical fibers in submarine cables can be deployed in very loosely bent (nearly straight) conditions, and the bend perturbations can be suppressed, which could suppress the random mode coupling. To investigate this, using the simulation method described in Section II, we numerically simulated the SMD of the CC-MCF after 1-km propagation, as a function of the fiber bend curvature. As shown in Fig. 16, the simulation results at the $f_{\mathrm{tw,pk}}$ of 3 and 5 turns/m agreed well with the measured results. In the simulation, the SMD was minimized at the bend curvature of around 2.5 m^{-1} (the R_{b} of around 40 cm), and the minimum SMD was about 2/3 of the SMD at the R_{b} of 31 cm. When the bend curvature was smaller than 2.5 m^{-1}, the SMD rapidly increased as the bend curvature approached 0 m^{-1}. Therefore, the CC-MCF design has to be further improved for enhancing the random coupling in the very loosely bent conditions.

V. Conclusion

The coupled-core multi-core fiber with four pure-silica cores achieved the record-low SMD of 3.14 $\pm$ 0.17 ps/$\sqrt{\text{km}}$ over C-band and the ultra-low average attenuation of 0.158 dB/km at 1550 nm. The attenuation comparable to the ultra-low-loss SMF will be able to realize the spatial channel increase without the degradation of the per-channel capacity. Furthermore, according to the theoretical studies [12], [13], the strong random mode coupling may result in much lower nonlinear noises than that in a SMF with the same core-mode $\mathrm{A_{eff}}$.

Though the MIMO calculation complexity may be a concern in the coupled-core/mode transmission system, the first real-time MIMO DSP demonstration over a CC-MCF was already reported in 2015 [32]. Revisiting the digital coherent DSP case, the 100-G digital coherent DSP chip was commercialized only three years after the first real-time digital coherent DSP demonstration [33]–[35].

The results in this paper demonstrate the strong applicability of the CC-MCF to the ultra-long-haul submarine transmission system with the limited valuable cross section of the cable. With the further design optimization of the CC-MCF and the research progress in the MIMO DSP field, the CC-MCF can become a strong and realistic candidate for the next-generation transmission fiber of the ultra-high-capacity ultra-long-haul transmission system.

References

[1] R.-J. Essiambre and R. W. Tkach, "Capacity trends and limits of optical communication networks," *Proc. IEEE*, vol. 100, no. 5, pp. 1035–1055, May 2012.

[2] A. Sano *et al.*, "102.3-Tb/s (224 $\times$ 548-Gb/s) C- and extended L-band all-Raman transmission over 240 km using PDM-64QAM single carrier FDM with digital pilot tone," in *Proc. Opt. Fiber Commun. Conf.*, 2012, Paper PDP5C.3.

[3] P. J. Winzer, "Scaling optical fiber networks: Challenges and solutions," *Opt. Photon. News*, vol. 29, no. 3, pp. 28–35, Mar. 2015.

[4] KDDI Corporation, "A global consortium to build new trans-pacific cable system 'FASTER," *News Release*, Aug. 11, 2014. [Online]. Available: http://news.kddi.com/kddi/corporate/english/newsrelease/2014/08/11/581.html. [Accessed: 24-Feb-2016].

[5] J.-X. Cai *et al.*, "64QAM based coded modulation transmission over transoceanic distance with >60 Tb/s capacity," in *Proc. Opt. Fiber Commun. Conf.*, 2015, Paper Th5C.8.

[6] J. X. Cai *et al.*, "54 Tb/s transmission over 9,150 km with optimized hybrid Raman-EDFA amplification and coded modulation," in *Proc. Eur. Conf. Opt. Commun.*, Cannes, France, 2014, Paper PD.3.3.

[7] T. Hayashi, Y. Tamura, T. Hasegawa, and T. Taru, "125-μm-cladding coupled multi-core fiber with ultra-low loss of 0.158 dB/km and record-low spatial mode dispersion of 6.1 ps/km$^{1/2}$," in *Proc. Opt. Fiber Commun. Conf.*, 2016, Paper Th5A.1.

[8] S. Randel *et al.*, "MIMO-based signal processing of spatially multiplexed 112-Gb/s PDM-QPSK signals using strongly-coupled 3-core fiber," in *Proc. Eur. Conf. Opt. Commun.*, Geneva, Switzerland, 2011, Paper Tu.5.B.1.

[9] T. Hayashi *et al.*, "Coupled-core multi-core fibers: High-spatial-density optical transmission fibers with low differential modal properties," in *Proc. Eur. Conf. Opt. Commun.*, Valencia, Spain, 2015, Paper We.1.4.1.

[10] R. Ryf *et al.*, "Space-division multiplexed transmission over 4200 km 3-core microstructured fiber," in *Proc. Opt. Fiber Commun. Conf.*, 2012, Paper PDP5C.2.

[11] K.-P. Ho and J. M. Kahn, "Mode-dependent loss and gain: Statistics and effect on mode-division multiplexing," *Opt. Express*, vol. 19, no. 17, pp. 16612–16635, Aug. 2011.

[12] G. P. Agrawal, S. Mumtaz, and R.-J. Essiambre, "Nonlinear performance of SDM systems designed with multimode or multicore fibers," in *Proc. Opt. Fiber Commun. Conf.*, 2013, Paper OM3I.6.

[13] C. Antonelli, M. Shtaif, and A. Mecozzi, "Modeling of nonlinear propagation in space-division multiplexed fiber-optic transmission," *J. Lightw. Technol.*, vol. 34, no. 1, pp. 36–54, Jan. 2016.

[14] M. Hirano *et al.*, "Record low loss, record high FOM optical fiber with manufacturable process," in *Proc. Opt. Fiber Commun. Conf.*, 2013, Paper PDP5A.7.

[15] S. Makovejs *et al.*, "Record-low (0.1460 dB/km) attenuation ultra-large Aeff optical fiber for submarine applications," in *Proc. Opt. Fiber Commun. Conf.*, 2015, Paper Th5A.2.

[16] H. Yamaguchi, Y. Yamamoto, T. Hasegawa, T. Kawano, M. Hirano, and Y. Koyano, "Ultra-low loss and large Aeff pure-silica core fiber advances," in *Proc. SubOptics*, Dubai, 2016, Paper EC07.

[17] T. Sakamoto, T. Mori, M. Wada, T. Yamamoto, F. Yamamoto, and K. Nakajima, "Fiber twisting and bending induced adiabatic/nonadiabatic super-mode transition in coupled multi-core fiber," *J. Lightw. Technol.*, vol. 34, no. 4, pp. 1228–1237, Feb. 2016.

[18] T. Hayashi *et al.*, "Effects of core count/layout and twisting condition on spatial mode dispersion in coupled multi-core fibers," in *Proc. Eur. Conf. Opt. Commun.*, Düsseldorf, Germany, 2016, pp. 559–561.

[19] S. Fan and J. M. Kahn, "Principal modes in multimode waveguides," *Opt. Lett.*, vol. 30, no. 2, pp. 135–137, Jan. 2005.

[20] B. E. Little and W.-P. Huang, "Coupled-mode theory for optical waveguides," *Prog. Electromagn. Res.*, vol. 10, pp. 217–270, 1995.

[21] ITU-T G.650.1, "Definitions and test methods for linear, deterministic attributes of single-mode fibre and cable," Jul. 2010.

[22] T. Hayashi, T. Taru, O. Shimakawa, T. Sasaki, and E. Sasaoka, "Uncoupled multi-core fiber enhancing signal-to-noise ratio," *Opt. Express*, vol. 20, no. 26, pp. B94–B103, Nov. 2012.

[23] Y. Tamura, T. Hayashi, T. Hasegawa, and T. Taru, "Large-Aeff uncoupled dual-core fiber with 125μm-diameter cladding (in Japanese with English title)," in *Proc. IEICE Commun. Soc. Conf. 2016*, 2016, Paper B-10-2.

[24] B. Costa, D. Mazzoni, M. Puleo, and E. Vezzoni, "Phase shift technique for the measurement of chromatic dispersion in optical fibers using LED's," *IEEE J. Quantum Electron.*, vol. 18, no. 10, pp. 1509–1515, Nov. 1982.

[25] ITU-T G.650.2, "Definitions and test methods for statistical and non-linear related attributes of single-mode fibre and cable," Aug. 2015.

[26] T. Hayashi, T. Taru, O. Shimakawa, T. Sasaki, and E. Sasaoka, "Characterization of crosstalk in ultra-low-crosstalk multi-core fiber," *J. Lightw. Technol.*, vol. 30, no. 4, pp. 583–589, Feb. 2012.

[27] A. H. Nuttall, "Some windows with very good sidelobe behavior," *IEEE Trans. Acoust. Speech Signal Process.*, vol. 29, no. 1, pp. 84–91, Feb. 1981.

[28] N. Gisin, R. Passy, and J. P. V. der Weid, "Definitions and measurements of polarization mode dispersion: interferometric versus fixed analyzer methods," *IEEE Photon. Technol. Lett.*, vol. 6, no. 6, pp. 730–732, Jun. 1994.

[29] R. Maruyama, N. Kuwaki, S. Matsuo, K. Sato, and M. Ohashi, "DMD free transmission line composed of TMFs with large effective area for MIMO processing," in *Proc. Eur. Conf. Opt. Commun.*, 2012, Paper Tu.1.F.2.

[30] T. Mori, T. Sakamoto, M. Wada, T. Yamamoto, and F. Yamamoto, "Low DMD four LP mode transmission fiber for wide-band WDM-MIMO system," in *Proc. Opt. Fiber Commun. Conf.*, Anaheim, CA, USA, 2013, Paper OTh3K.1.

[31] T. Mori, T. Sakamoto, M. Wada, T. Yamamoto, and F. Yamamoto, "Six-LP-mode transmission fiber with DMD of less than 70 ps/km over C+L band," in *Proc. Opt. Fiber Commun. Conf.*, 2014, Paper M3F.3.

[32] S. Randel *et al.*, "First real-time coherent MIMO-DSP for six coupled mode transmission," in *Proc. IEEE Photon. Conf.*, Reston, VI, USA, 2015, pp. 1–2, doi: 10.1109/IPCon.2015.7323761.

[33] T. Pfau *et al.*, "Real-time synchronous QPSK transmission with standard DFB lasers and digital I&Q receiver," in *Proc. Opt. Amplifiers Their Appl./Coherent Opt. Technol. Appl.*, 2006, Paper CThC5.

[34] Nortel Networks Corporation, "Nortel unveils industry's first commercially available 100G optical solution," Press Release, Dec. 14, 2009. [Online]. Available: http://www.marketwired.com/press-release/nortel-unveils-industrys-first-commercially-available-100g-optical-solution-1090143.htm. [Accessed: 24-Feb-2016].

[35] Verizon Inc., "Verizon deploys commercial 100G ultra-long-haul optical system on portion of its core European network," Press Release, Dec. 14, 2009. [Online]. Available: http://www.prnewswire.com/news-releases/verizon-deploys-commercial-100g-ultra-long-haul-optical-system-on-portion-of-its-core-european-network-79213242.html. [Accessed: 24-Feb-2016].

Tetsuya Hayashi (M'10) received the B.E. and M.E. degrees in electronic engineering from the University of Tokyo, Tokyo, Japan, in 2004 and 2006, respectively, and the Ph.D. degree in engineering from Hokkaido University, Sapporo, Japan, in 2013.

In 2006, he joined Optical Communications Laboratory, Sumitomo Electric Industries, Ltd., Yokohama, Japan. He has been engaged in research and development on optical fibers and fiber optics. He is the author of a book chapter, "Multi-core optical fibers," in *Optical Fiber Telecommunications* (Elsevier, 2013).

Dr. Hayashi is a Member of the Institute of Electronics, Information, and Communication Engineers (IEICE) of Japan, and the Optical Society of America. He received the 2009 IEICE Young Researcher's Award, 2011 IEICE Communication Society OCS Young Researchers Award, and 2012 IEICE Communication Society OCS Best Paper Award.

Yoshiaki Tamura received the B.E. and M.E. degrees in chemical engineering from the University of Osaka, Suita, Japan, in 2006 and 2008, respectively.

In 2008, he joined Optical Communications Laboratory, Sumitomo Electric Industries, Ltd., Yokohama, Japan, and since then he has been engaged in research and development of optical fibers.

Mr. Tamura is a Member of the Institute of Electronics, Information, and Communication Engineers of Japan. He received the 31st Kenjiro Sakurai Memorial Prize (2016) from the Optoelectronics Industry and Technology Development Association of Japan.

Takemi Hasegawa (M'14) received the B.E. and M.E. degrees in electronic engineering from the University of Tokyo, Tokyo, Japan, in 1997 and 1999, respectively.

In 1999, he joined Sumitomo Electric Industries (SEI), Ltd., Yokohama, Japan. He has been engaged in research and development on optical fibers and photonic sensors. From 2015, he is working as a Group Manager with Optical Communications Laboratory of SEI, and involved in research and development on single-mode optical fibers.

Toshiki Taru received the M.E. degree in metallurgical engineering from the University of Tokyo, Tokyo, Japan, in 1997.

He joined in 1997 and is currently working as a Group Manager with Optical Communications Laboratory, Sumitomo Electric Industries, Ltd., Yokohama, Japan, where he has been working on research and development of optical fibers and fiber optic components. From 2005 to 2007, he was a Visiting Researcher with the University of Bath where he conducted the research on all-solid photonic-crystal fibers. From 2013 to 2015, he was with New Business Development Division, SEI.